Assessing Control of Fixed-Support Balance Recovery in Wearable Lower-Limb Exoskeletons Using Multibody Dynamic Modelling

Keaton A. Inkol and John McPhee

***Abstract*— Despite many lower-limb exoskeletons requiring the use of crutches to maintain upright postures, limited research has assessed control of standing balance recovery in these systems. Using a model-based approach, the current simulation study investigated the performance of impedance controllers designed to assist with standing fixed-support balance recovery. A novel multibody dynamic model of the integrated human-exoskeleton system was designed to move in the sagittal plane. Development of the exoskeleton model (Technaid Exo-H3) was accompanied by parameter identification. The balancing torques produced by the human in the model were derived from offline linear control methods and saturated to approximate the torque-production of a young individual either with or without incomplete spinal cord injury. Without intervention, the injured user was not able to recover upright posture following a forward push of specific magnitude. Thus, three feedback control laws, inspired by robotics research (exoskeletons and humanoids), were implemented in the simulated exoskeleton. Each law assisted with balance recovery via reference tracking within the joint and/or whole-body center of mass space. Following optimization of control parameters, all proposed exoskeleton control laws were successful in assisting the injured user return to an upright posture. Joint space control yielded the best joint-level reference tracking during recovery, while center of mass control better reduced forward center of mass excursions — albeit at the cost of joint-level tracking accuracy.**

I. INTRODUCTION

For many individuals with mobility deficits, such as those who have experienced a spinal cord injury (SCI), active wearable exoskeletons provide an opportunity to regain independence. These systems can allow the user to execute various motor tasks (e.g. sit-to-stand and walking) with a level of assistance tuned to their specific needs [1], [2]. However, a major concern in using these robotic systems is the stability of upright postures [3], [4]. Often, crutches, which limit a user's ability to perform activities of daily living stress-free, are necessary to maintain balance. Additionally, control methods such as finite-state architectures, often employed in state-of-the-art exoskeletons [2], can induce balance-loss by perturbing the system during periods of state transition.

Methods of standing balance control used within wearable exoskeletons are typically based upon observations from human experiments. For example, Horak and Nashner [5] disseminated the use of ankle and hip strategies for balance recovery following external perturbations. The former involves inverted pendulum control of posture; the latter consists of anti-phase ankle (plantarflexion) and hip (flexion) rotations. Recently, Rajasekaran et al. [6] proposed a promising assist-as-needed control method that could aid both ankle and hip strategies through joint angle-dependent stiffness and stability limits. Emmens et al. [4] and [7] subsequently introduced exoskeleton control of quiet standing and fixed-support balance recovery using classical proportional-derivative (PD) control of whole-body center of mass (COM). Assisted balance recovery in the COM-task space, as opposed to the joint space, draws parallels to popular biomechanical models of feedback stance control in humans [8], [9], [10]. While Emmens demonstrated the capabilities of their system in restoring balance control in select individuals with SCI (i.e. unable to balance unassisted), the exoskeleton output torques were limited to driving only the ankle and knee joints.

Multibody dynamic modelling of the integrated (or combined) human-exoskeleton system is limited within the literature. Relatively few models exist of wearable lower-limb exoskeletons that both span multiple joints and are integrated with whole-body human dynamics [3], [11], [12]. Modelling and simulation of the integrated human-exoskeleton system provides an opportunity to refine device/controller design (and more) without putting an individual's health, or the hardware being tested, at risk, i.e., "model-in-loop" simulation.

The purpose of the current study is twofold: i) design a symbolic multibody model of the integrated human-exoskeleton system; ii) assess the performance of exoskeleton feedback control in assisting with multi-joint (ankle, knee, and hip) balance recovery. Specifically, the model was used to gauge the capabilities of techniques employed in nonlinear tracking control of robotic systems (computed torque control; CTC), to expand the current body of knowledge surrounding assisted standing balance control [4], [6], [7]. A separate controller, with no knowledge of the embedded exoskeleton controller, generated human torques for the case of an individual with and without (*control*) incomplete SCI. The goal was to then have the exoskeleton controller assist the SCI user from falling (following a push) by driving them towards the *control* user's joint/COM trajectories.

II. INTEGRATED HUMAN-EXOSKELETON MODEL

Multibody dynamic models of the Technaid® Exo-H3 wearable exoskeleton (Technaid S.L., Madrid, Spain), and the human user (Fig. 1), were designed in MapleSim (Maplesoft, Waterloo, Canada). The dynamics of both models, when kinematically constrained together, were an integrated system

*This work was funded by the Canada Research Chairs Program (J.M) and the Natural Sciences and Engineering Research Council of Canada and University of Waterloo (K.A.I)

Keaton A. Inkol and John McPhee are with the Department of Systems Design Engineering, University of Waterloo, 200 University Ave W, Canada kainkol@uwaterloo.ca

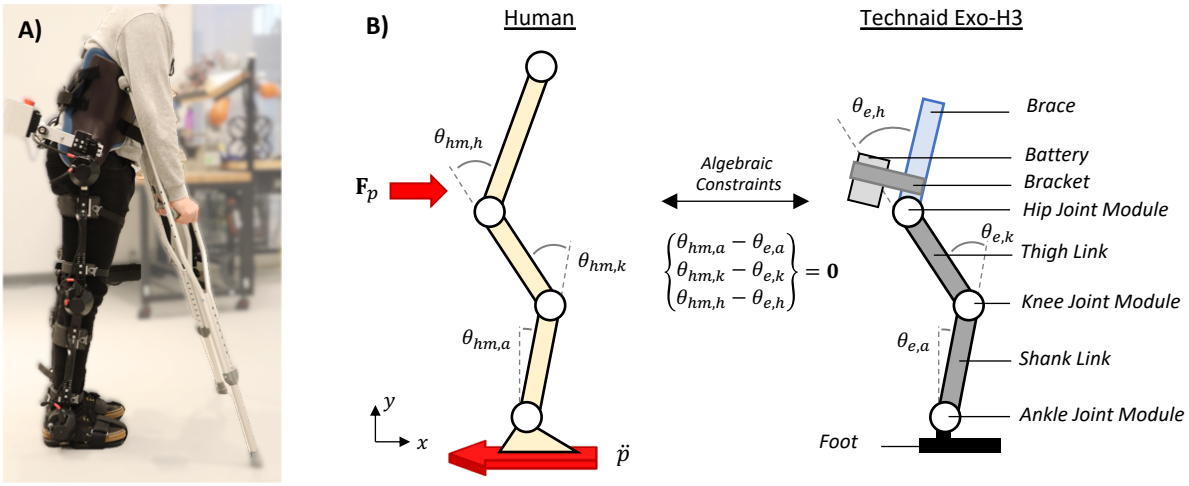

Fig. 1. A) Image of an individual wearing the Technaid Exo-H3 and B) schematics of the planar multibody human and exoskeleton model. Red arrows indicate the two types of perturbations that could be applied to the model; push perturbations $\mathbf{F}_p$ (used in the current study) and support-surface accelerations $\ddot{p}$. Also indicated are the human and exoskeleton ankle, knee, and hip angles ($\{\theta_{\cdot,a}, \theta_{\cdot,k}, \theta_{\cdot,h}\}$) and exoskeleton rigid bodies (shown in *italics*).

of differential-algebraic equations (DAEs):

$$\begin{bmatrix}\mathbf{M} & -\mathbf{J}_q^T\\ \mathbf{J}_q & \mathbf{0}\end{bmatrix}\begin{Bmatrix}\ddot{\mathbf{q}}\\ \boldsymbol{\lambda}\end{Bmatrix}=\begin{Bmatrix}\boldsymbol{\Gamma}(\mathbf{q},\dot{\mathbf{q}})+\mathbf{P}(\mathbf{q},\mathbf{F}_p,\ddot{p})+\boldsymbol{\tau}_{in}\\ -\dot{\mathbf{J}}_q\dot{\mathbf{q}}-2\alpha\dot{\boldsymbol{\Phi}}-\beta^2\boldsymbol{\Phi}\end{Bmatrix} \quad (1)$$

where $\mathbf{M}$ is the inertia matrix, $\boldsymbol{\Gamma}$ returns gravitational, velocity-dependent, and passive joint torques, and $\boldsymbol{\tau}_{in}$ is the concatenation of the input torques from the human and exoskeleton $\boldsymbol{\tau}_{in} = \{\boldsymbol{\tau}_{hm}, \boldsymbol{\tau}_e\}^T$. Additionally, the function $\mathbf{P}$ maps perturbation forces $\mathbf{F}_p$ (push to sacrum) and support-surface accelerations $\ddot{p}$ to torques. The generalized coordinates $\mathbf{q} = \{\mathbf{q}_{hm}, \mathbf{q}_e\}^T$ describe sagittal plane rotations of the ankle, knee, and hip joints for the human ($\{\theta_{hm,a}, \theta_{hm,k}, \theta_{hm,h}\}$; $\mathbf{q}_{hm} \in \mathbb{R}^3$) and exoskeleton ($\{\theta_{e,a}, \theta_{e,k}, \theta_{e,h}\}$; $\mathbf{q}_e \in \mathbb{R}^3$).

The human and Exo-H3 models were fixed together using algebraic constraint equations [13],

$$\boldsymbol{\Phi}=\begin{Bmatrix}\theta_{hm,a}-\theta_{e,a}\\ \theta_{hm,k}-\theta_{e,k}\\ \theta_{hm,h}-\theta_{e,h}\end{Bmatrix}=\mathbf{0} \quad (2)$$

which emulate the ideal scenario in which the exoskeleton and human joint centers are perfectly aligned [14]. This simplification bypassed the need for additional model elements and any related parameters [15]. The relevant reaction torques (Lagrange multipliers, $\boldsymbol{\lambda}$) that maintained the constraints (2) were evaluated using the constraint Jacobian $\mathbf{J}_q = \partial\boldsymbol{\Phi}/\partial\mathbf{q}$ with Baumgarte stabilization. This method uses the coefficients α and β to provide PD-like control of constraint violations during integration of DAEs.

A. Lower-Limb Exoskeleton Model

The Technaid Exo-H3 consists of two leg modules in addition to a trunk segment (brace, bracket and battery). Brushless DC motors actuate the ankle, knee, and hip joint, within the sagittal plane (3 degrees of freedom per leg; DOF), over the following ranges of motion: ankle (30° of plantar- and dorsiflexion); knee (105° flexion, 5° extension); hip (105° flexion, 30° extension). Rotary encoders are fixed to each joint to provide joint angles in real-time, while pressure sensors in each foot segment provide information regarding center of pressure movement (COP).

The model of the Exo-H3 consisted of a single point mass (the battery fixed to the trunk segment) and 8 rigid bodies (Fig. 1b): 3 motorized joint modules (contain joint, motor and gearbox); 2 stainless steel links connecting joints in series; 1 foot segment fixed to the support-surface; the brace/orthosis that secures the user's trunk in the exoskeleton; and the bracket/attachment from which the battery is fixed. For this preliminary version, the legs were assumed to behave symmetrically and motors acted as ideal torque actuators.

The multibody parameters identified for the Exo-H3 are listed in Table I. Note the values listed are for a single component; since the right and left legs were lumped together, inertial and torque properties were doubled in the model. The mass of each rigid body was measured using a scale calibrated to 4 kg. To approximate the moment of inertia and center of mass location for each rigid body of interest, a moment of inertia tester was used (MOI-025-004, Inertia Dynamics, USA). All joint modules were assumed to have equivalent inertia; the same was assumed for the inertia of links between joint. Moreover, the inertia of each joint module was based on measurements from the ankle segment alone. Position of the battery and trunk brace, in the trunk reference frame, were based on measurements following fitting of the exoskeleton to an individual 1.80 m in height (body mass = 75 kg).

The damping resulting from the exo-actuators and joints was estimated using a commercial dynamometer (Biodex System 4 Pro, Biodex, USA). Specifically, the Exo-H3 was fixed to the dynamometer seat and motion of the knee joint was isolated and recorded at 100 Hz. The knee was moved at a constant velocity $\dot{\theta}_e = \{2, 4, 10, 20, 45\}$ deg s^{-1} over the

interval $[0, -\pi/2]$ rad, where the knee was fully extended at 0 rad (see Fig. 1b). The torques recorded for each velocity condition were windowed over the periods of constant velocity and filtered using a zero-lag dual-pass filter (2^{nd} order low-pass Butterworth, cut-off = 20 Hz). Torques resulting from gravity were removed from the processed data. The nonlinear least squares curve fitting function `lsqnonlin` (MATLAB, USA) was subsequently used to fit the processed passive torques, across each velocity, to the affine damping function

$$\tau_{e,p} = y - D_e\dot{\theta}_e \tag{3}$$

where y was the torque measured at zero speed. The linear component of Eq. (3) was implemented in the Exo-H3 model. It was assumed that each joint had identical damping D_e and that joint impedance was identical between the two directions of rotations. To avoid the effects of bias during the curve-fitting process, each velocity condition was provided the same number of data points within the tested range of motion. The results of the curve-fitting procedure are shown in Fig. 2. Note that due to abnormalities in the passive torques measured during knee flexion (e.g. large jumps in torque between neighbouring joint angles), the current study utilized data collected only during knee extension.

B. Human Biomechanical Model

The human-user model paired with the lower-limb exoskeleton also consisted of three DOF (identical to those of the exoskeleton). Upper limb rigid bodies were present in the model but fixed in anatomical position, similar to that instructed in balance recovery studies [4], [16]. The segment properties necessary to formulate the model dynamics (mass, length, moment of inertia, and COM position) were scaled according to the height and weight of the individual to be simulated (height = 1.80 m, weight = 75), via the Winter [8] anthropometric tables. These values are omitted from the current manuscript due to document length limitations.

To reduce computational costs related to muscle modelling, the dynamics of the human model were entirely torque-driven. Passive moments resulting from viscoelastic structures (e.g. muscle connective tissue, joint capsule, etc.) were included to factor into controller design. Lower limb joint stiffness was based on the empirically-derived coupled exponential stiffness equations from Riener and Edrich [17]. These equations consider the effects of biarticular musculature on the resulting joint impedance. Lastly, a linear torsional damper with the damping coefficient $c = 0.1$ Nm rad^{-1} was fixed to each joint [18].

C. Control-Oriented Dynamics

To design the Exo-H3 balance recovery controllers, the constraint equations (2) were dropped from (1); the equations of motion were then rewritten in terms of $\mathbf{q}_e$ as ordinary differential equations (i.e. (2) was always true).

For control of the human within the exoskeleton, the intent was to derive a controller that would not have knowledge of the exoskeleton's intent (similar to a novice user), and would not drastically increase computation times when incorporated into an optimization procedure. Thus, the nonlinear dynamics (1) were written entirely in terms of $\mathbf{q}_{hm}$ and linearized in state-space. The state was $\mathbf{x} = \{\mathbf{q}_{hm}, \dot{\mathbf{q}}_{hm}\}$, and for *any* desired static configuration $\mathbf{x}_d = \{\mathbf{q}_d, \dot{\mathbf{q}}_d\}$, the dynamics of the human-exoskeleton system could be written as

$$\dot{\mathbf{x}} = \mathbf{A}\mathbf{x}_{er}(t) + \mathbf{B}\boldsymbol{\tau}_{er}(t) \tag{4}$$

where $\mathbf{x}_{er}(t) = \mathbf{x}(t) - \mathbf{x}_d$ and $\boldsymbol{\tau}_{er}(t) = \boldsymbol{\tau}_{hm}(t) - \boldsymbol{\tau}_d$. Given the nonlinear dynamics $\dot{\mathbf{x}} = \mathbf{f}(\cdot)$ from (1),

$$\mathbf{A} = \left.\frac{\partial \mathbf{f}}{\partial \mathbf{x}_{er}}\right|_{\substack{\mathbf{x}=\mathbf{x}_d \\ \boldsymbol{\tau}=\boldsymbol{\tau}_d}}, \quad \mathbf{B} = \left.\frac{\partial \mathbf{f}}{\partial \boldsymbol{\tau}_{er}}\right|_{\substack{\mathbf{x}=\mathbf{x}_d \\ \boldsymbol{\tau}=\boldsymbol{\tau}_d}} \tag{5}$$

Note that the desired torques $\boldsymbol{\tau}_d$ were inputs that fulfilled static equilibrium: $\mathbf{f}(\mathbf{x}_d, \boldsymbol{\tau}_d) = \mathbf{0}$.

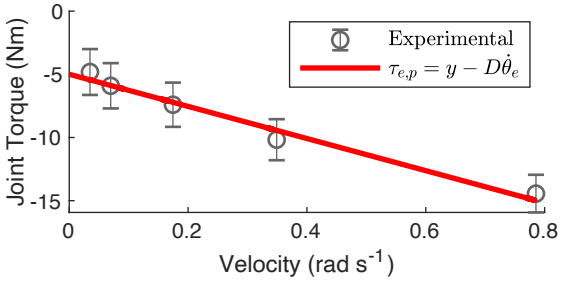

Fig. 2. Results of fitting Eq. (3) to the passive torques measured in the Exo-H3 knee joint. Experimental data, shown as the mean torque across the joint angles spanned for each velocity (○; error bars indicate ±1 SD), was analyzed only for the positive/extension direction of knee velocity.

TABLE I
PARAMETERS MEASURED FOR THE TECHNAID EXO-H3 RIGID BODIES.

Parameter	Value
Joint Module Param.	
D_e (Nm rad^{-1})	12.8
Mass (kg)	1.39
M.o.i (kg m^2)	1.69E-3
Link Param.	
Mass (kg)	9.30E-2
M.o.i (kg m^2)	7.22E-4
Miscellaneous Inertia Param.	
Foot mass (kg)	0.62
Battery mass (kg)	2.78
Brace mass (kg)	1.39
Brace m.o.i (kg m^2)	9.39E-2
Bracket mass (kg)	1.36
Bracket m.o.i (kg m^2)	3.36E-2
*Segment COM Position** $[x, y]$	
Brace COM (m)	[-0.22, 0.10]
Battery COM (m)	[-0.25, 0.10]

*Expressed in trunk frame

III. HUMAN MODEL CONTROL & SIMULATION

A. Feedback Control Law

Control of the human model was based on a linear quadratic regulator (LQR; Fig. 3). Using the control-oriented linearized equation (4), an optimal set of gains $\mathbf{K}_{hm}$ could be derived. These gains minimized a cost function that was

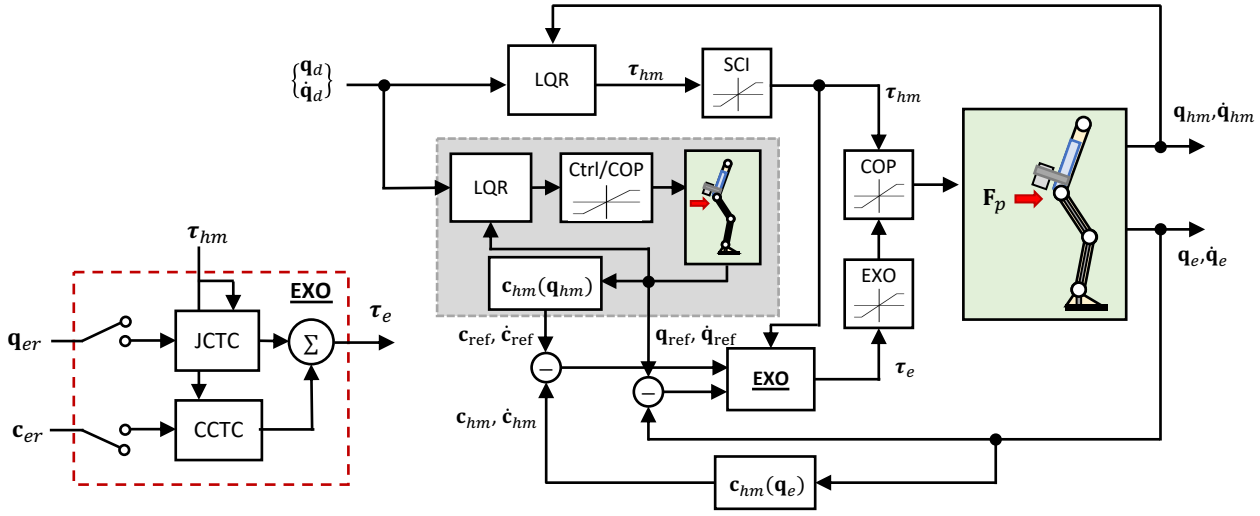

Fig. 3. Block diagram of the integrated human-and-exoskeleton balance recovery system for the SCI user (note the torque saturation blocks). The dashed grey region shows how the LQR and control-user (Ctrl) saturation limits generate reference trajectories for the exoskeleton balance controller (EXO).The details of switching between the EXO controllers (JCTC, CCTC, COMB) are highlighted in the dashed red area.

quadratic in both $\mathbf{x}$ and $\boldsymbol{\tau}_{hm}$. The resulting feedback torques were,

$$\boldsymbol{\tau}_{hm} = \mathbf{K}_{hm}(\mathbf{x}_d - \mathbf{x}) + \boldsymbol{\tau}_d \tag{6}$$

The matrix $\mathbf{Q}$ included in the LQR cost function (*not shown*) was based on a first-order Taylor series of the horizontal COM position, as done previously for the control of a double pendulum [19]. Additionally, the $\mathbf{R}$ matrix required for the LQR formulation was set to identity.

B. Control User vs. SCI User Simulations

For each simulation, the model was initialized at the *static*, zero velocity fixed/desired point $\mathbf{q}_e(0) = \mathbf{q}_d = \{0.052, 0, 0\}^T$ rad. This configuration provided a human COM equilibrium position similar to that observed during experimental stance [20]. Simulations spanned a two-second window to allow for complete balance recovery (return to $\mathbf{x}_d$) [7], [16]. A fixed-step explicit trapezoidal method was used to integrate the system forward; this method reduced the time required within the gain optimization procedure (see IV-D), while minimizing the numerical inaccuracies intrinsic to lower-order methods. The control user was modelled by imposing saturation limits on $\boldsymbol{\tau}_{hm}$ according to the maximal isometric torques reported in [21] (Table II). To then have a simple model of a user that behaves like an individual with an incomplete SCI, control torque saturation limits were scaled by 40% [22]. Ankle torques were also saturated when the COP exceeded the base of support boundaries, according to the linearized COP approximation in [8].

To estimate the performance of the control and SCI users with no assistance from the exoskeleton, the integrated model was simulated forward in response to a push perturbation. A *horizontal* force was applied superior to the hip joint (5 cm) using the function,

$$F_{p,x} = \begin{cases} P \sin\left(\frac{\pi t}{T}\right) & \text{if } t < T \\ 0 & \text{else} \end{cases} \tag{7}$$

which mimicked the force profiles in [7]. Parameters P and T were the peak magnitude and duration of force applied, respectively. To determine the threshold at which the SCI user could not recover (while the control user still could), T was set to 225 ms, and P was progressively increased from 0. At $P = 380$ N (Impulse $= 54.4$ N·sec), the SCI could no longer recover balance (see Fig. 4). Thus, the exoskeleton controllers described in the following section aimed to stabilize the SCI user for this magnitude of perturbation by tracking the stable control-user trajectories as reference.

IV. EXOSKELETON CONTROLLER DESIGN & SIMULATION

A. Computed Torque Control: Joint Space (JCTC)

In the exoskeleton joint space, it's feasible to derive a nonlinear control law to stabilize certain configurations and trajectories using CTC (i.e. JCTC). In the current study, the intent was to assist the SCI user in tracking what was considered their desired/reference motor plans (based on the performance of the control user).

Control about the reference (control user) balance recovery trajectory took the form,

$$\boldsymbol{\tau}_e = \mathbf{M}(\mathbf{K}_j\mathbf{q}_{er} + \mathbf{D}_j\dot{\mathbf{q}}_{er}) - \boldsymbol{\Gamma}(\mathbf{q}_e, \dot{\mathbf{q}}_e) - \boldsymbol{\tau}_{hm} \tag{8}$$

where $\mathbf{q}_{er} = \mathbf{q}_{\text{ref}} - \mathbf{q}_e$, $\dot{\mathbf{q}}_{er} = \dot{\mathbf{q}}_{\text{ref}} - \dot{\mathbf{q}}_e$, and $\mathbf{K}_j$ and $\mathbf{D}_j$ are coupled stiffness and damping matrices respectively. Inherently, this control method provides both a feedforward torque, to compensate for quadratic velocity effects and gravitational toppling, and feedback torque to correct for any deviations from the referenced LQR states. Additionally, it is assumed that the controller can reasonably estimate $\boldsymbol{\tau}_{hm}$ via the interaction torque sensors shipped with the Exo-H3.

TABLE II

OUTPUT TORQUE SATURATION LIMITS FOR THE LUMPED LOWER-LIMBS.

Joint Torque	[Lower Limit, Upper Limit]
$\tau_{hm,a}$ (Nm)	[-252, 88]
$\tau_{hm,k}$ (Nm)	[-230, 431]
$\tau_{hm,h}$ (Nm)	[-426, 300]
τ_{e_i} (Nm)	[-290, 290]

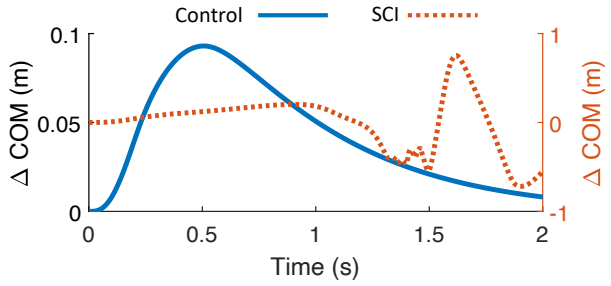

Fig. 4. Balance recovery COM trajectories (ΔCOM w.r.t. COM equilibrium point) following a push perturbation ($P = 380$ N) using the control (blue) and SCI (orange; right y-axis) torque saturation limits. The reduced torque limits provided to the SCI user prevented the LQR controller from stabilizing the fixed-point resulting in divergence.

B. Computed Torque Control: COM Space (CCTC)

As human balance recovery is typically framed within the context of the COM task-space, it is of interest to formulate a nonlinear feedback law within that space (CCTC). For a k rigid-body system, the COM position is evaluated as

$$\text{COM} \equiv \mathbf{c} = \frac{1}{M}\sum_{i=1}^{k} m_i \mathbf{c}_{s,i}(\mathbf{q}) \tag{9}$$

where M is the system's total mass; m_i and $\mathbf{c}_{s,i}$ are the i^{th} segment mass and COM position. To create better synergy between the exoskeleton and human controllers, the COM was evaluated for only the human ($\mathbf{c}_{hm}$) (see III-A) [7], [4].

By using the Jacobian $\mathbf{J}_c = \partial \mathbf{c}_{hm}/\partial \mathbf{q}_e$, such that,

$$\dot{\mathbf{q}}_e = \mathbf{J}_c^{-1}\dot{\mathbf{c}}_{hm} \tag{10}$$

$$\ddot{\mathbf{q}}_e = \mathbf{J}_c^{-1}(\ddot{\mathbf{c}}_{hm} - \dot{\mathbf{J}}_c\dot{\mathbf{q}}_e) \tag{11}$$

where $\mathbf{J}_c^{-1}$ is the damped least-squares pseudoinverse, the open-chain equations of motion can be written in COM-space:

$$\mathbf{J}_c^T\mathbf{F}_c = \mathbf{M}\mathbf{J}_c^{-1}(\ddot{\mathbf{c}}_{hm} - \dot{\mathbf{J}}_c\dot{\mathbf{q}}_e) - \boldsymbol{\Gamma}(\mathbf{q},\dot{\mathbf{q}}) - \boldsymbol{\tau}_{hm} \tag{12}$$

$$\mathbf{F}_c = \mathbf{J}_c^{-T}[\mathbf{M}\mathbf{J}_c^{-1}(\ddot{\mathbf{c}}_{hm} - \dot{\mathbf{J}}_c\dot{\mathbf{q}}_e) - \boldsymbol{\Gamma}(\mathbf{q},\dot{\mathbf{q}}) - \boldsymbol{\tau}_{hm}] \tag{13}$$

where $\mathbf{J}_c^{-T} \equiv (\mathbf{J}_c^T)^{-1}$. From this result, an impedance-like force applied to the COM ($\mathbf{F}_c^*$) can be derived:

$$\begin{aligned}\mathbf{F}_c^* = {} & \mathbf{J}_c^{-T}[\mathbf{M}\mathbf{J}_c^{-1}(\mathbf{K}_c\mathbf{c}_{er} + \mathbf{D}_c\dot{\mathbf{c}}_{er} - \dot{\mathbf{J}}_c\dot{\mathbf{q}}_e)] \\ & - \mathbf{J}_c^{-T}[\boldsymbol{\Gamma}(\mathbf{q},\dot{\mathbf{q}}) + \boldsymbol{\tau}_{hm}]\end{aligned} \tag{14}$$

where $\mathbf{c}_{er} = \mathbf{c}_{\text{ref}} - \mathbf{c}_{hm}$, $\dot{\mathbf{c}}_{er} = \dot{\mathbf{c}}_{\text{ref}} - \dot{\mathbf{c}}_{hm}$, and $\mathbf{K}_c$ and $\mathbf{D}_c$ are now gain matrices in COM space. Once evaluated, $\mathbf{F}_c^*$ can then be mapped back to $\boldsymbol{\tau}_e$.

C. Computed Torque Control: Combined (COMB)

Alternatively, the controller implemented in the exoskeleton can combine both the JCTC and CCTC feedback laws through summation (COMB). This method is similar to that employed in a humanoid COM control architecture [23]. Here, the authors combined joint-space LQR with a CTCC controller (controlled only horizontal COM position) to stabilize a static upright posture following a push. The joint-space torques provide restoration to a specific postural configuration, while the COM torques can generate human-like counterbalance strategies, e.g. the hip strategy [5], [19], [23]. Note that feedforward terms are included only once within the combined system.

D. Controller Optimization

The control systems JCTC and CCTC should be theoretically stable assuming the gains are set appropriately. For the current paper, an optimization-based approach was used to select these for the SCI user specifically. The system was simulated again over a two-second span, in which the exoskeleton controller was not active until $t = 250$ ms; this was approximately where the SCI and control trajectories diverged (Fig. 4). This allowed the SCI user-model to handle the initial feedback response. At each joint, boundaries were imposed on $\boldsymbol{\tau}_e$ to keep it below the motors' momentary peak torque, as specified by the Exo-H3 manufacturer (Table II). If the COP exceeded the base of support boundaries during simulation, the ankle motor would try to generate a counter-torque to maintain the COP at the corresponding boundary.

The gains that minimized the cost function,

$$J = \frac{w_1}{\Pi_1}(\delta\mathbf{X}_f \cdot \delta\mathbf{X}_f) + \int_0^2 \left[\frac{w_2}{\Pi_2}(c_x - c_{eq})^2 + \frac{w_3}{\Pi_3}\dddot{c}_x^2\right] dt \tag{15}$$

were determined via a shooting method. The cost function (15), inspired by previous research [16], [19], consisted of a terminal cost dependent on the final state, $\delta\mathbf{X}_f = \mathbf{x}_d - \{\mathbf{q},\dot{\mathbf{q}}\}|_{t=2}$, and an integral component that measured the displacement of the horizontal COM position from its equilibrium point (i.e. ΔCOM; $c_{eq} = 0.05$ m, [20]) in addition to COM jerk $\dddot{c}_x$ (for smooth trajectories). Each term was normalized using a factor Π_i; its value was based on evaluations of each term when using the control-user LQR alone. The following set of weights were used: w_1 = 2; w_2 = 1; w_3 = 1.

The optimal control problem was initially solved using particle swarm optimization. Multiple iterations were executed to increase the likelihood of converging upon a global optimum within the search space. The solutions from particle swarm were then fine-tuned using gradient-based optimization (`fmincon` in MATLAB). Controllers were quantitatively assessed according to the peak ΔCOM [7], as well as the root mean square error between the control and assisted COM (RMSC; horizontal component only) and joint angle trajectories (RMSJ) . The latter (RMSJ) was averaged across the ankle, knee, and hip joints. Based on the LQR feedback gains, as well as trial-and-error, elements in the gain matrices were bounded between -2000 and 2×10^4. All

TABLE III

OUTCOME MEASURES FOR THE PROPOSED EXO-H3 CONTROLLERS.

Outcome	JCTC	CCTC	COMB
Peak ΔCOM (m)	0.121	0.118	0.121
RMSC (m)	0.034	0.019	0.031
RMSJ (rad)	0.129	0.162	0.141

computations were performed using an Intel Core i7 CPU (3.60 GHz) and 16.0 GB of memory.

V. RESULTS AND DISCUSSION

Using LQR to control the human in the exoskeleton yielded a combined hip/knee strategy rather than a strict double pendulum-like strategy (locked-knee); however, the results were reasonably human-like regardless [24] (Fig. 5). Displacements of the COM were still acceptable relative to human experiments (ΔCOM $\approx$ 8 cm in [16]; ΔCOM $=$ 9.5 cm in the current study, Fig. 5) and were always within the base of support boundaries. The impulse required to destabilize the SCI user in the current study was much larger than the tolerance of the individuals with SCI in [7], where the fall-threshold was 30 N·sec. The result was a larger ΔCOM (>10 cm) for assisted balance recovery relative to reported outcomes from the exoskeleton literature [4], [7]; however, the two-second window of recovery was very similar to [7]. Despite these differences, the limits imposed on the SCI user in the current study were successful in differentiating it from the control user, such that assistive control was necessary for balance recovery. Improved model predictions will require refinement of the details surrounding the effects of SCI on motor control.

Fig. 5 and Table III highlight the performance of each controller following the push perturbation. On average, each two-second simulation required 0.66 CPU seconds. All controllers were successful in assisting the SCI user recover balance and return towards their desired static posture. Using JCTC yielded the best joint level tracking (lowest RMSJ) in addition to smooth recovery kinematics. However, using CCTC reduced the peak ΔCOM experienced by the simulated user, yielded better tracking of the control COM (lowest RMSC), and brought the COM closer to the equilibrium point after 2 seconds (relative to JCTC). Some non-ideal oscillations were evident in the CCTC joint trajectories and the hip experienced a greater deal of hip flexion (reflected by the large RMSJ), which remained after 2 seconds. These issues may have been due to inaccuracies in the mapping by the damped pseudoinverse Jacobian, which should be refined in the future. Lastly, using COMB produced similar results to the JCTC — both qualitatively and quantitatively. With that said, at the end of the simulated horizon, the COMB controller appeared to drive the COM past its equilibrium point. This overshoot can be observed in the joint angles as well (ankle and knee). Hypothetically, this underdamped behaviour may be the result of the JCTC and CCTC competing to stabilize the same configuration. This strategy may bring

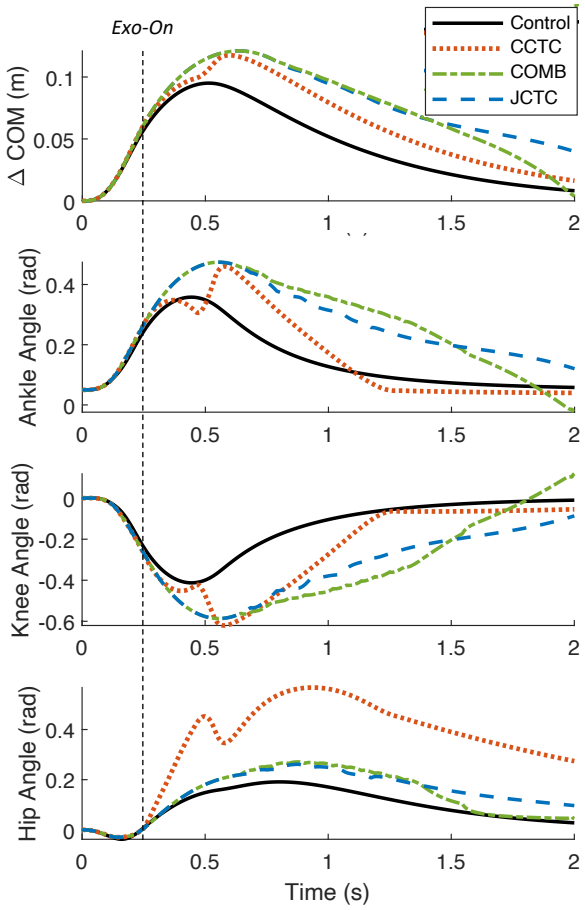

Fig. 5. Performance of the three exoskeleton balance recovery controller variations (JCTC, CCTC, COMB) in assisting the SCI user following push onset (at $t = 0$). The instant at which the exoskeleton controller is turned on is labelled "Exo-On". Note: positive ankle angle is dorsiflexion; positive knee angle is extension; positive hip angle is flexion.

the COM towards its equilibrium point quicker than JCTC alone (while avoiding the abrupt changes in direction seen with CCTC), but does not allow one to infer stability without setting longer simulation times.

In the current study, a fixed time determined the onset of exoskeleton assistance to limit the number of variables that could determine each controller's success. Realistically, some variable(s) that reflects stability of the system could be substituted [6], [10], [9]. Ideally, the exoskeleton balance controller should be capable of transitioning between different recovery strategies (e.g. transition from ankle to hip strategy) to improve robustness against a multitude of perturbation modalities [5]. This may require definition of various control laws, according to movements within joint, COM and COP space, and validation against multiple perturbation types, e.g. support-surface accelerations.

Given the nature of this simulation-based research, it is important to identify the limitations and areas upon which to improve. Foremost, validation of the current motion predictions was limited to outcomes reported within the literature; experimental validation of controllers will be necessary within future work. The human model will be

given additional details including musculoskeletal elements that impose biological constraints (e.g. muscles [21]), and more adept controllers that reflect characteristics of the central nervous system, e.g. process delays, tracking subject-specific reference trajectories. Furthermore, the human LQR implemented in the current study was not able to recognize and adjust its control strategy with knowledge of limits in COP position, torque limits [19], and the torques applied by the exoskeleton. These would be features of learned responses by the nervous system; the latter would come with practice using the exoskeleton [25].

The exoskeleton model will also be improved upon in the future. This will primarily involve the inclusion of actuator dynamics and characterization of the aforementioned joint module impedance nonlinearities ignored in the current study. Additionally, rather than assuming ideal conditions (i.e. Eq. (2)), the effects of human-exoskeleton interface compliance on force transmission, for which there seems to be limited simulation research [15], [14], should be identified. Lastly, for the foot-ground interactions, we assumed no slipping and used a simple COP approximation [8]; therefore, a stricter domain of admissible motions should be prescribed for the integrated human-exoskeleton model in the future.

VI. CONCLUSION

The current study provided a preliminary simulation analysis in which variations of computed torque control (CTC) laws were shown to *assist* a model of an exoskeleton end user (with SCI) in executing balance recovery. To the authors' knowledge, this is the first demonstration of exoskeleton standing balance recovery via CTC; thus, this limited area of the literature has been expanded [4], [6], [7]. How dynamic simulations can benefit researchers in the design of assistive devices and controllers was also highlighted, i.e. testing scenarios in which falls can occur without worry of harm to the user/participant. In the future, the aim is to utilize the perturbation labs at the University of Waterloo [26], to assess performance of the proposed exoskeleton balance recovery systems in both healthy and clinical/rehabilitation users.

ACKNOWLEDGMENT

Thank you to Dr. James Tung for assistance during parameter identification of the Exo-H3.

REFERENCES

[1] G. Lv, H. Zhu, and R. D. Gregg, "On the Design and Control of Highly Backdrivable Lower-Limb Exoskeletons: A Discussion of Past and Ongoing Work," *IEEE Control Syst. Mag.*, vol. 38, no. 6, pp. 88–113, Dec. 2018.

[2] M. R. Tucker, J. Olivier, A. Pagel, H. Bleuler, M. Bouri, O. Lambercy, J. d. R. Milln, R. Riener, H. Vallery, and R. Gassert, "Control strategies for active lower extremity prosthetics and orthotics: a review," *J. NeuroEng. Rehabil.*, vol. 12, no. 1, p. 1, 2015.

[3] O. Harib, A. Hereid, A. Agrawal, T. Gurriet, S. Finet, G. Boeris, A. Duburcq, M. E. Mungai, M. Masselin, A. D. Ames, K. Sreenath, and J. W. Grizzle, "Feedback Control of an Exoskeleton for Paraplegics: Toward Robustly Stable, Hands-Free Dynamic Walking," *IEEE Control Syst. Mag.*, vol. 38, no. 6, pp. 61–87, Dec. 2018.

[4] A. R. Emmens, E. H. F. van Asseldonk, and H. van der Kooij, "Effects of a powered ankle-foot orthosis on perturbed standing balance," *J. NeuroEng. Rehabil.*, vol. 15, no. 1, p. 50, 2018.

[5] F. B. Horak and L. M. Nashner, "Central programming of postural movements: adaptation to altered support-surface configurations," *J. Neurophysiol.*, vol. 55, no. 6, pp. 1369–1381, 1986.

[6] V. Rajasekaran, J. Aranda, A. Casals, and J. L. Pons, "An adaptive control strategy for postural stability using a wearable robot," *Rob. Auton. Syst.*, vol. 73, pp. 16–23, Nov. 2015.

[7] A. Emmens, E. van Asseldonk, M. Masciullo, M. Arquilla, I. Pisotta, N. L. Tagliamonte, F. Tamburella, M. Molinari, and H. van der Kooij, "Improving the Standing Balance of Paraplegics through the Use of a Wearable Exoskeleton," in *2018 7th IEEE Int. Conf. Biomed. Robot. and Biomechatron. (Biorob)*, Aug. 2018, pp. 707–712.

[8] D. A. Winter, *Biomechanics and motor control of human movement*, 4th ed. Hoboken, N.J: Wiley, 2009, oCLC: ocn318408191.

[9] A. L. Hof, M. G. J. Gazendam, and W. E. Sinke, "The condition for dynamic stability," *J. Biomech.*, vol. 38, no. 1, pp. 1–8, 2005.

[10] K. A. Inkol and L. Vallis, "Modelling the dynamic margins of stability for use in evaluations of balance following a support-surface perturbation," *J. Biomech.*, 2019.

[11] H. Koch and K. Mombaur, "ExoOpt - A framework for patient centered design optimization of lower limb exoskeletons," in *2015 IEEE Int. Conf. Rehabil. Robot. (ICORR)*, Aug. 2015, pp. 113–118.

[12] E. P. Grabke, K. Masani, and J. Andrysek, "Lower Limb Assistive Device Design Optimization Using Musculoskeletal Modeling: A Review," *J. Med. Devices*, vol. 13, no. 4, p. 040801, 2019.

[13] M. Millard, M. Sreenivasa, and K. Mombaur, "Predicting the Motions and Forces of Wearable Robotic Systems Using Optimal Control," *Front. Rob. AI*, vol. 4, p. 41, 2017.

[14] M. Cenciarini and A. M. Dollar, "Biomechanical considerations in the design of lower limb exoskeletons," in *2011 IEEE Int. Conf. Rehabil. Robot. (ICORR)*, June 2011, pp. 1–6.

[15] M. C. Sanchez-Villaman, D. Torricelli, and J. L. Pons, "Modeling Human-Exoskeleton Interaction: Preliminary Results," in *Wearable Robotics: Challenges and Trends*, M. C. Carrozza, S. Micera, and J. L. Pons, Eds. Cham: Springer International Publishing, 2019, vol. 22, pp. 137–141.

[16] C. S. Versteeg, L. H. Ting, and J. L. Allen, "Hip and ankle responses for reactive balance emerge from varying priorities to reduce effort and kinematic excursion: A simulation study," *J. Biomech.*, vol. 49, no. 14, pp. 3230–3237, 2016.

[17] R. Riener and T. Edrich, "Identification of passive elastic joint moments in the lower extremities," *J. Biomech.*, vol. 32, no. 5, pp. 539–544, 1999.

[18] G. T. Yamaguchi, *Dynamic modeling of musculoskeletal motion: a vectorized approach for biomechanical analysis in three dimensions*. Berlin: Springer, 2006, oCLC: 150263239.

[19] A. D. Kuo, "An optimal control model for analyzing human postural balance," *IEEE Trans. Biomed. Eng.*, vol. 42, no. 1, pp. 87–101, 1995.

[20] A. Karlsson and H. Lanshammar, "Analysis of postural sway strategies using an inverted pendulum model and force plate data," *Gait Posture*, vol. 5, no. 3, pp. 198–203, 1997.

[21] D. E. Anderson, M. L. Madigan, and M. A. Nussbaum, "Maximum voluntary joint torque as a function of joint angle and angular velocity: model development and application to the lower limb," *J. Biomech.*, vol. 40, no. 14, pp. 3105–3113, 2007.

[22] A. Jayaraman, C. M. Gregory, M. Bowden, J. E. Stevens, P. Shah, A. L. Behrman, and K. Vandenborne, "Lower extremity skeletal muscle function in persons with incomplete spinal cord injury," *Spinal Cord*, vol. 44, no. 11, pp. 680–687, 2006.

[23] B. Stephens, "Integral control of humanoid balance," in *2007 IEEE/RSJ Int. Conf. Intell. Robots and Systems*, Oct. 2007, pp. 4020–4027.

[24] A. V. Alexandrov, A. A. Frolov, F. B. Horak, P. Carlson-Kuhta, and S. Park, "Feedback equilibrium control during human standing," *Biol. Cybern.*, vol. 93, no. 5, pp. 309–322, 2005.

[25] E. H. F. van Asseldonk, A. Emmens, T. J. H. Brug, I. Pisotta, M. Arquilla, F. Tamburella, M. Masciullo, N. L. Tagliamonte, R. Valette, M. Molinari, and H. van der Kooij, "Training Balance Recovery in People with Incomplete SCI Wearing a Wearable Exoskeleton," in *Wearable Robotics: Challenges and Trends*, M. C. Carrozza, S. Micera, and J. L. Pons, Eds. Cham: Springer International Publishing, 2019, vol. 22, pp. 334–338.

[26] T. B. Winberg, "The Effects of Varying Surface Translation Acceleration and Velocity on Compensatory Forward Stepping Responses," Master's thesis, Dept. Kin., Univ. Waterloo, Waterloo, Canada, 2018.